

# **Zr<sup>4+</sup>-Doped Anatase TiO<sub>2</sub> Nanotube Array Electrode for Electrocatalytic Reduction of L-cystine**

**Weizhen Wang, Guangxin Wang, Xuhui Zhao \*, Xiaofeng Zhang, Yuming Tang \* and Yu Zuo**

Beijing Key Laboratory of Electrochemical Process and Technology for Materials, Beijing University of Chemical Technology, Beijing 100029, China;

**Abstract:** A Zr<sup>4+</sup>-doped anatase TiO<sub>2</sub> nanotube array electrode was prepared using a process that included Ti anodizing, chemical immersion, and heat treatment. The compositions, microstructure, and electrochemical properties of the prepared electrodes were characterized. The results show that Zr<sup>4+</sup> was successfully introduced into the TiO<sub>2</sub> nanotube array electrodes. Because Zr<sup>4+</sup> was doped into the crystal structure of the TiO<sub>2</sub> and replaced a part of Ti<sup>4+</sup> to form more oxygen vacancies and Ti<sup>3+</sup>, the electrocatalytic activity of the prepared electrodes, for the reduction of L-cystine, was significantly improved.

**Keywords:** nanocomposites; oxidation; titanium dioxide; electrocatalysis

## **1. Introduction**

L-cysteine is widely used in many fields, such as medicine, cosmetics, and biochemical research. The typical industrial production of L-cysteine is achieved through the electrocatalytic reduction of L-cystine. The currently used Pb electrodes, or other catalytic electrodes with deposited Pb, are prone to heavy metal pollution in acid electrolytes. Although titanium electrodes have also been used in the reduction of L-cystine, the effect is not satisfactory [1]. Therefore, developing alternative materials with stable performance, that are environmentally friendly and have a high catalytic reduction activity, are one of the current research hotspots [2–4].

As one of the most studied catalytic materials, TiO<sub>2</sub> has an important role in the field of catalysis [5–11]. Skúlason et al. [12] discussed the role of transition metal oxides in the electrocatalytic reduction of N<sub>2</sub> by using density functional theory (DFT) calculations. Hirakawa et al. [13] reported the role of oxygen vacancies and Ti<sup>3+</sup> in TiO<sub>2</sub> in the photocatalytic reduction of N<sub>2</sub>. In order to enhance the catalytic activity of TiO<sub>2</sub>, doping metal elements are used to increase the vacancies and defects in the TiO<sub>2</sub> crystal structure [14–17]. At present, most of the correlative research in this field mainly focuses on the photocatalysis of TiO<sub>2</sub>. However, there are relatively few studies on its electrocatalysis, especially regarding electrocatalytic reduction. Recently, Cao et al. [18,19] reported in detail that a Zr<sup>4+</sup>-doped TiO<sub>2</sub> electrode can efficiently reduce N<sub>2</sub> through electrocatalysis. This provides a feasible idea from which we can design a TiO<sub>2</sub> nanotube array electrode with a high electrocatalytic reduction activity for reducing L-cystine. Moreover, considering the better stability of titanium and the existence of the oxygen vacancies and Ti<sup>3+</sup> in the anatase TiO<sub>2</sub>, the TiO<sub>2</sub> nanotube array electrode might also possess good potential in the field of electrocatalytic reduction.

We have designed a Zr<sup>4+</sup>-doped anatase TiO<sub>2</sub> nanotube array electrode (anatase Zr/TiO<sub>2</sub>), in which Zr<sup>4+</sup> partly replaces Ti<sup>4+</sup> in the anatase TiO<sub>2</sub>, and studied its electrocatalytic reduction activity for reducing L-cystine and discussed its reduction mechanism.

We have designed a Zr<sup>4+</sup>-doped anatase TiO<sub>2</sub> nanotube array electrode (anatase Zr/TiO<sub>2</sub>), in which Zr<sup>4+</sup> partly replaces Ti<sup>4+</sup> in the anatase TiO<sub>2</sub>, and studied its electrocatalytic reduction activity

2020, 3572 2 of 7 for reducing L-cystine and discussed its reduction mechanism.

## 2. Materials and Methods

### 2. Materials and Methods

The preparation process for the anatase Zr/TiO<sub>2</sub> electrode is shown in Figure 1a. Firstly, the TiO<sub>2</sub> nanotube arrays on the pure Ti foil (99.99 wt%) surface was prepared through anodizing, which was carried out in 35 wt% (CH<sub>2</sub>OH)<sub>2</sub> (ethylene glycol) + 0.5 wt% HF (hydrofluoric acid) solutions, under a constant voltage of 20 V for 35 min at room temperature. The auxiliary electrode was a graphite. After anodization, the samples were soaked in deionized water and then chemically immersed in a 0.3 mol L<sup>-1</sup> Zr(NO<sub>3</sub>)<sub>4</sub> solution for 4 h, in order to dope Zr<sup>4+</sup>. Subsequently, the samples were washed with deionized water and ethanol, several times. Finally, they were heated to 450 °C, kept for two hours, and cooled slowly in a muffle furnace.

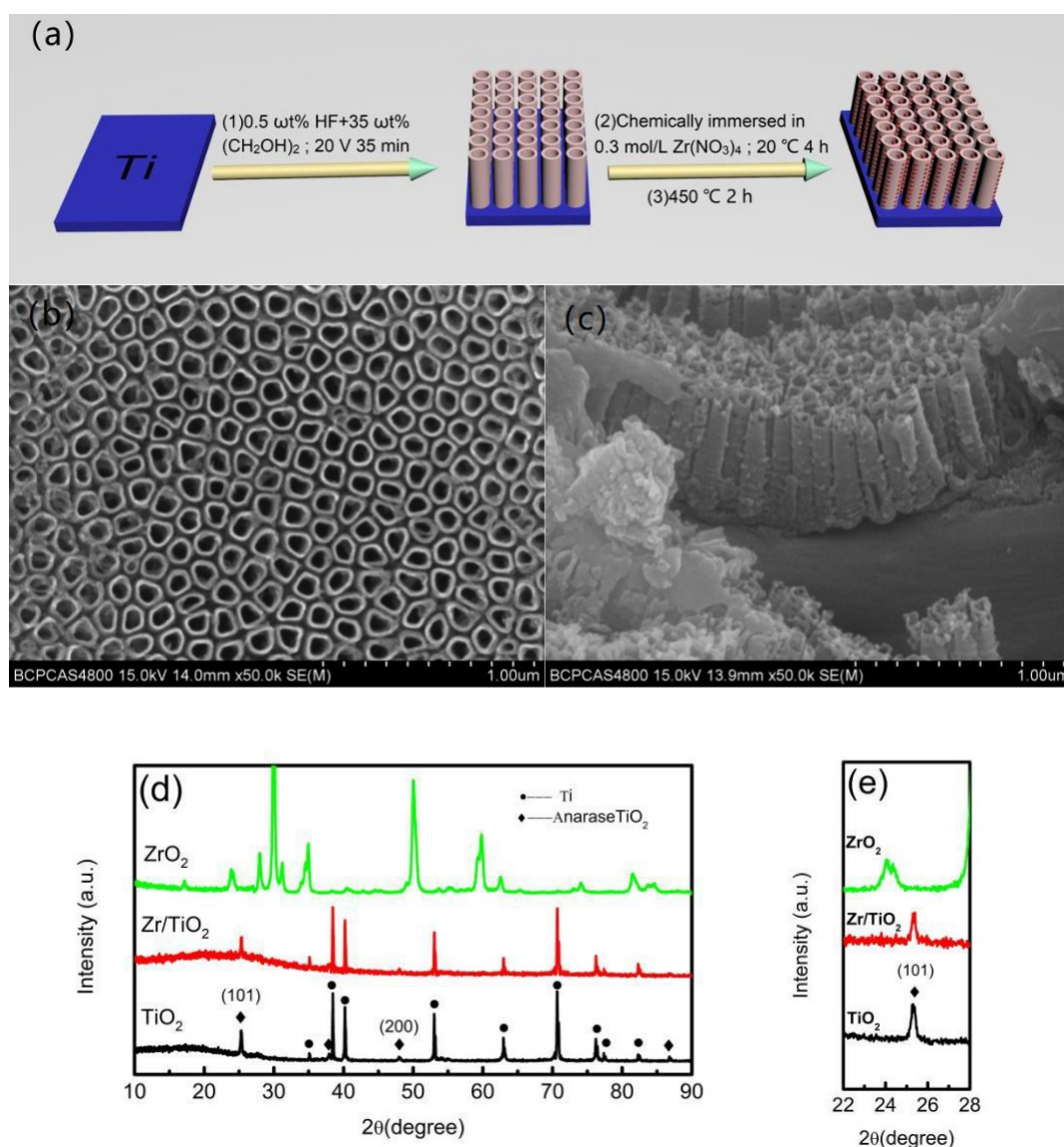


**Figure 1.** Preparation process (a), surface (b), and section (c) morphologies, and XRD patterns (d,e) of

**Figure 1.** Preparation process (a), surface (b), and section (c) morphologies, and XRD patterns (d,e) of anatase Zr/TiO<sub>2</sub> nanotube array electrode.

anatase Zr/TiO<sub>2</sub> nanotube array electrode.

The crystal structure of the modified electrode surface was studied using X-ray diffraction (XRD)

The crystal structure of the modified electrode surface was studied using X-ray diffraction (XRD) (Bruker D8 advance, Cu K $\alpha$ ,  $\lambda$  = 0.1548 nm, Berlin, Germany). The morphology, length, and diameter

(Bruker D8 advance, Cu K $\alpha$ ,  $\lambda$  = 0.1548 nm, Berlin, Germany). The morphology, length, and diameter of the TiO<sub>2</sub> nanotubes on the electrode surface were characterized using a SEM (S-4800, Hitachi,

Tokyo, Japan). The existence and valence of Ti and Zr on the surface of the Zr/TiO<sub>2</sub> electrode were characterized using X-ray photoelectron spectroscopy (XPS) (PHI 1600 ESCA, PerkinElmer, Waltham,

MA, USA). The binding energies of the peaks were calibrated using the binding energy of the C1s peak (285 eV).

The electrochemical performance was tested using the electrochemical workstation (CS350H, Wuhan Corrtest, Wuhan, China). In the three-electrode system, the auxiliary electrode was a Pt electrode, and the reference electrode was a saturated calomel electrode. The test solutions were HCl solutions containing L-cystine.

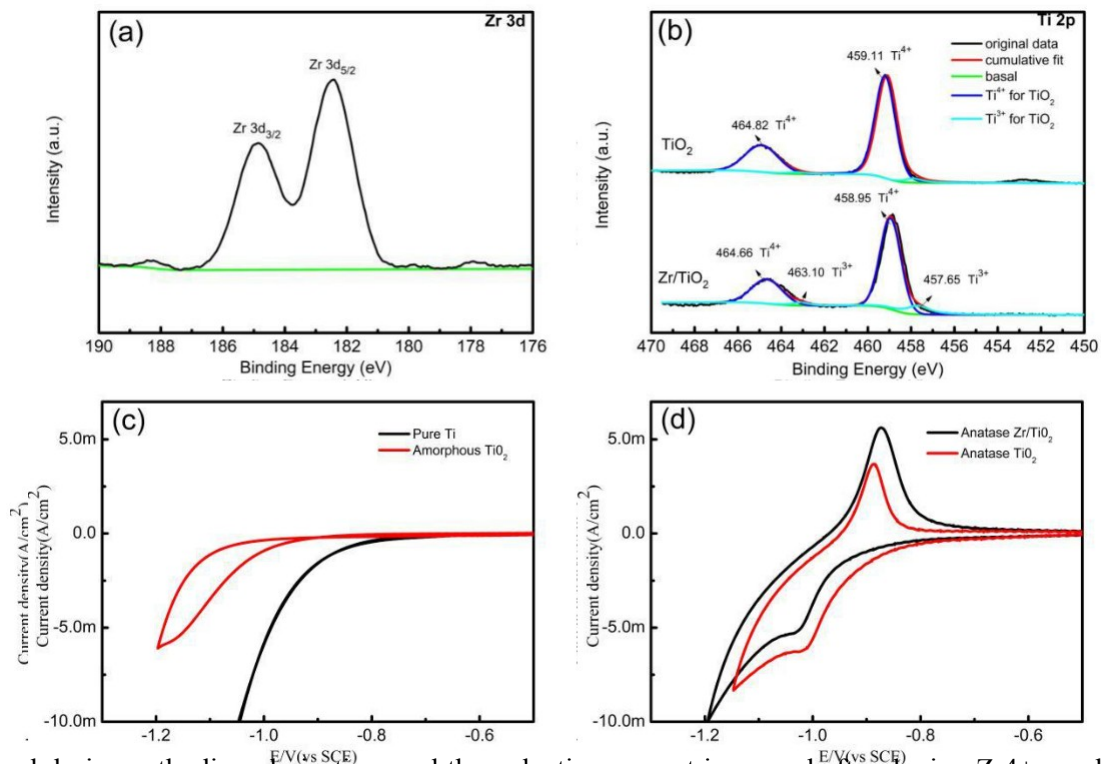
### 3. Results

Scanning electron microscopy (SEM) images show that the anatase Zr/TiO<sub>2</sub> electrode has a tubular structure, with tube diameters and lengths of about 100 and 650 nm, respectively (Figure 1b,c). The crystalline structures of the different samples were studied using X-ray diffraction (Figure 1d)—for both the undoped and Zr<sup>4+</sup>-doped TiO<sub>2</sub> nanotube arrays. The other diffraction peaks correspond to the anatase phase (JCPDS # 21-1272). A close examination of the pattern (Figure 1e), after doping Zr<sup>4+</sup>, revealed that the peak intensity of the TiO<sub>2</sub> slightly decreased. According to the Scherrer equation, the calculated grain sizes of the TiO<sub>2</sub> (101) were about 7 and 5.1 nm for the undoped and doped samples, respectively, suggesting that the grain sizes of the TiO<sub>2</sub> also became slightly smaller after doping Zr<sup>4+</sup>. Above, the results indicate that the crystallinity of the TiO<sub>2</sub> slightly decreased. No diffraction peak relating to the ZrO<sub>2</sub> was observed in the XRD pattern (JCPDS # 79-1768). Compared to Ti<sup>4+</sup>, Zr<sup>4+</sup> is suitable in size, and is similar in d electron configuration and oxide structure (Zr<sup>4+</sup> 72 pm, Ti<sup>4+</sup> 52 pm) [15]. Zr<sup>4+</sup> was doped into the anatase TiO<sub>2</sub> to replace a part of Ti<sup>4+</sup>, and did not change the anatase crystal structure [18].

X-ray photoelectron spectroscopy (XPS) was used to characterize the chemical composition of the electrode surface. Figure 2 shows an overview of the XPS spectra for the undoped and Zr<sup>4+</sup>-doped TiO<sub>2</sub> nanotube array electrodes. The Zr<sup>4+</sup>-doped electrode surface is mainly composed of Ti and O, containing a small amount of Zr (about 2.44 atom. %). The peak of C1s may be attributed to the contaminants on the sample surface. In addition, the binding energies of the peaks were calibrated by the binding energy of the C1s peaks (285 eV). The Zr 3D spectra (Figure 3a) show two obvious peaks, revealing that the Zr element was on the surface of the electrode. However, there was no diffraction peak of ZrO<sub>2</sub> in the XRD pattern (Figure 1d), and the peak intensity of the TiO<sub>2</sub> slightly decreased; its peak positions moved slightly to the right after the doping of Zr<sup>4+</sup> (Figure 1e), indicating that the Zr should be incorporated into the TiO<sub>2</sub> crystal lattice [20,21]. Figure 3b shows the deconvoluted XPS spectrum for the Ti 2p region. From the XPS-peak-differentiating analysis, it was found that, regardless of Zr<sup>4+</sup>-doping or not, Ti<sup>3+</sup> and Ti<sup>4+</sup> exist in the TiO<sub>2</sub> electrodes. The four peaks correspond to the Ti<sup>3+</sup> 2p<sub>3/2</sub> (457.65 eV), Ti<sup>4+</sup> 2p<sub>3/2</sub> (458.95 eV), Ti<sup>3+</sup> 2p<sub>1/2</sub> (463.10 eV), and Ti<sup>4+</sup> 2p<sub>1/2</sub> (464.66 eV) [20]. However, for the undoped TiO<sub>2</sub> nanotube array electrode, the Ti<sup>3+</sup> content is very small (about 4.9 atom% of the total Ti). For the Zr<sup>4+</sup>-doped electrode, there is a significant increase in the area of two Ti<sup>3+</sup> sub-peaks in Figure 3b, indicating an increase in the Ti<sup>3+</sup> content (about 14.1 atom% of the total Ti). Compared with Figure 3c,d, the onset potential of the amorphous TiO<sub>2</sub> nanotube array electrode for a hydrogen evolution reaction (HER) is significantly more negative than that of the pure titanium electrode, but no other redox peak was observed in the cyclic voltammeteries (CVs) for both electrodes. However, for the undoped and Zr<sup>4+</sup>-doped anatase TiO<sub>2</sub> nanotube array electrodes, there were nearly reversible redox peaks in the CVs, which corresponded to a transformation between Ti<sup>4+</sup> and Ti<sup>3+</sup> [22]. Moreover, after doping Zr<sup>4+</sup>, the oxidation peak current decreased, and reduction peak current increased, which indicated that it is beneficial to transform Ti<sup>4+</sup> into Ti<sup>3+</sup> on the anatase Zr/TiO<sub>2</sub> nanotube array electrode. This is consistent with the previous XPS results.



**Figure 2.** XPS spectra of TiO<sub>2</sub> nanotube array surface: (a) Zr<sup>4+</sup> doped; (b) undoped.



found during cathodic polarization, and the reduction current increased after doping Zr<sup>4+</sup>, as shown in Figure 4c,d. This indicates that the anatase structure of TiO<sub>2</sub> is helpful in the formation of Ti<sup>3+</sup>, and in Figure 4c,d. This indicates that the anatase structure of TiO<sub>2</sub> is helpful in the formation of Ti<sup>3+</sup>, and

as shown in Figure 4c,d. This indicates that the anatase structure of TiO<sub>2</sub> is helpful in the formation of Ti<sup>3+</sup>, and the dopant of Zr<sup>4+</sup> can accelerate the transformation of Ti<sup>4+</sup> to Ti<sup>3+</sup>. Moreover, when adding

*Materials* **2020**, *13*, x FOR PEER REVIEW 5 of 7 L-cystine to HCl solutions, the reduction currents increase in the two anatase TiO<sub>2</sub> nanotube array electrodes, before hydrogen evolution is observed, which suggests that the anatase TiO possesses the the dopant of Zr<sup>4+</sup> can accelerate the transformation of Ti<sup>4+</sup> to Ti<sup>3+</sup>. Moreover, when adding 2 L-cystine electrocatalytic to HCl solutions, activities the reduction to reduce currents L-cystine increase. Compared in the two with anatase the undoped TiO<sub>2</sub> nanotube electrode, array electrothereductions,

current on the Zr<sup>4+</sup>-doped electrode has a more obvious increase, and the maximum difference in before hydrogen evolution is observed, which suggest that the anatase TiO<sub>2</sub> possesses the

current electrocatalytic (1.38 mA cm<sup>-2</sup>) activities<sup>2</sup> is about to reduc 2.26 times L-cystine that of. Compared the undoped with electro the undoped (0.61 mA cm<sup>-2</sup>) the<sup>2</sup>, reduction These results

current on the 4+ Zr<sup>4+</sup>-doped electrode has a more obvious increase, and the maximum difference in prove that the Zr -doped TiO<sub>2</sub> nanotube array electrode has good electrocatalytic reduction activity

current (1.38 mA cm<sup>-2</sup>) is about 2.26 times that of the undoped electrode (0.61 mA cm<sup>-2</sup>). These results for reducing L-cystine. In order to illustrate the effect of the Zr dopant content, the electrocatalytic

prove that the Zr<sup>4+</sup>-doped TiO<sub>2</sub> nanotube array electrode has good electrocatalytic reduction activity activity of the electrodes prepared in the different concentrations of Zr(NO<sub>3</sub>)<sub>4</sub> solution during the

for reducing L- cystine. In order to illustrate the effect of the Zr dopant content, the electrocatalytic chemical immersion process was studied using LSV, as shown in Figure 4e. From Figure 4e, the higher

activity of the electrodes prepared in the different concentrations of Zr(NO<sub>3</sub>)<sub>4</sub> solution during the

the concentrations of the Zr(NO<sub>3</sub>)<sub>4</sub> solution, the higher the electrocatalytic reduction activity of the chemical immersion process was studied using LSV, as shown in Figure 4e. From Figure 4e, the



prepared electrode. This implies that the amount of Zr dopant increases with increasing concentrations higher the concentrations of the  $Zr(NO_3)_4$  solution, the higher the electrocatalytic reduction activity of  $Zr(NO_3)_4$  solution, from 0.15 to 0.30 mol L<sup>-1</sup>. However, compared to the 0.30 mol L<sup>-1</sup>  $Zr(NO_3)_4$  prepared electrode. This implies that the amount of Zr dopant increases with increasing

3 4 solution, concentration of the electrocatalytic of  $Zr(NO_3)_4$  solution, activity from 0.15 to 0.30 mol L<sup>-1</sup>. However, prepared compared in the 0.45 to 0.30 mol L<sup>-1</sup>  $Zr(NO_3)_4$  solution, obviously the electrocatalytic improved. Figure 4f shows activity schematic of the electrode diagram prepared of the catalytic the 0.45 mol L<sup>-1</sup> reduction -1

$Zr(NO_3)_4$  solution was not obviously. Figure 4f shows a schematic diagram of the improved  $Zr^{4+}$  catalytic  $Zr^{4+}$  mechanism that reduces L-cystine on the  $Zr^{4+}$ -doped  $TiO_2$  nanotube array electrode. Because  $Zr^{4+}$  has reduction mechanism that reduces L-cystine on the  $Zr^{4+}$ -doped  $TiO_2$  nanotube array  $Zr^{4+}$  electrode.

a similar d electron configuration and oxide structure to but larger ionic size than Ti<sup>4+</sup>, doping  $Zr^{4+}$  Because  $Zr^{4+}$  has a similar d electron configuration and oxide structure to but larger ionic size than  $Ti^{4+}$  could not alter the crystalline structure of the anatase  $TiO_2$ , but it did create the stress therein [15].

$Ti^{4+}$ , doping  $Zr^{4+}$  could not alter the crystalline structure of the anatase  $TiO_2$ , but it did create the stress. The strained effect induced the formation and enrichment of the adjacent bi- $Ti^{3+}$ , which also resulted therein [15]. The strained effect induced the formation and enrichment of the adjacent bi- $Ti^{3+}$ , which

in the increased oxygen vacancies. These are beneficial to the enhancement of active centers [15,16]. also resulted in the increased oxygen vacancies. These are beneficial to the enhancement of active

The  $Ti^{3+}$  ions have a stronger attraction to the S atom of L-cysteine, to induce the S=S bond to break centers [15,16]. The  $Ti^{3+}$  ions have stronger attraction to the S atom of L-cysteine, to induce the S=S

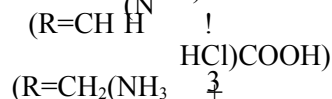
down. Therefore, doping  $Zr^{4+}$  improves the electrocatalytic activity of the anatase  $TiO_2$  nanotube array bond to break down. Therefore, doping  $Zr^{4+}$  improves the electrocatalytic activity of the anatase  $TiO_2$

electrode nanotube before the array reduction electrode of for L-cystine the reduction. of L-cystine.

L-cystine is not compatible with water, but it is easily soluble in acidic solutions. The reaction

equation for the dissolution of fit of

doublets double sulfur bond structure in aa HCl solution is [1]: [1]:



The anatase  $TiO_2$  has oxygen vacancies and Ti<sup>3+</sup> under a negative potential polarization. The reaction equation is [1]:

The anatase  $TiO_2$  has oxygen vacancies and Ti<sup>3+</sup> under a negative potential polarization. The reaction equation is [1]:  $TiO_2 + 4H^+ + e^- \rightarrow Ti^{3+} + 2H_2O$  (2)

Under the negative potential polarization, the  $Ti^{3+}$  reacts with the dissolved  $RSSR \cdot HCl$  in solution, as follows:

Under the negative potential polarization, the  $Ti^{3+}$  reacts with the dissolved  $RSSR \cdot HCl$  in the solution, as follows:



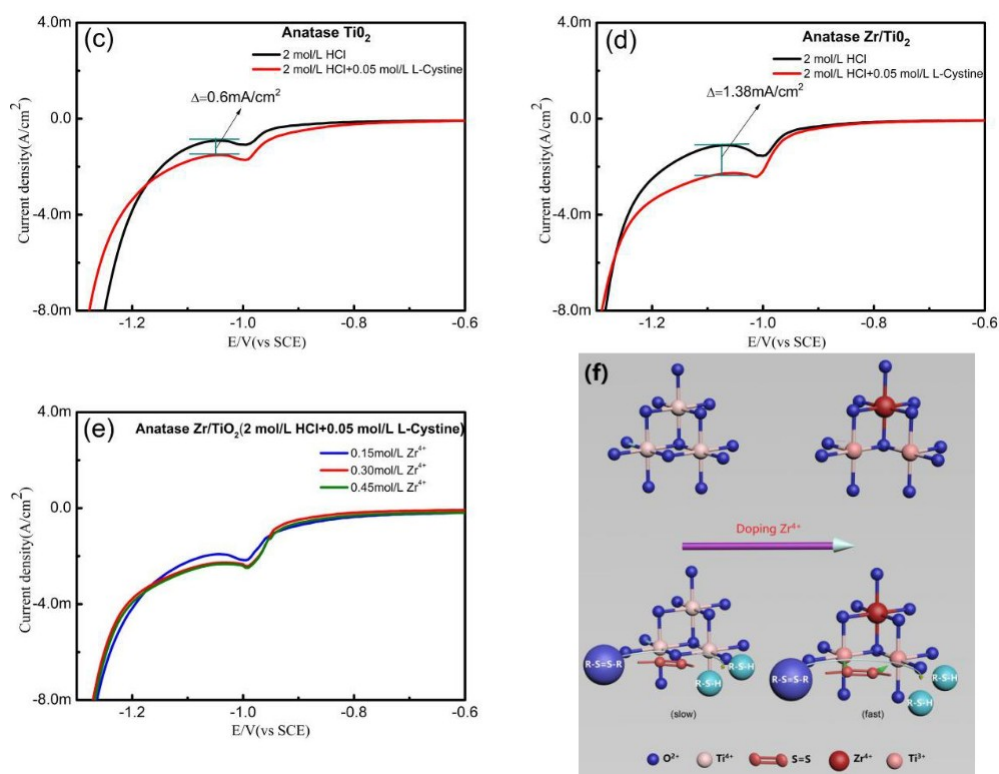


**Figure 4.** Linear sweep voltammetry (LSV) curves of different electrodes in 2 mol/L HCl or 2 mol/L HCl + 0.05 mol/L L-cystine solutions (scan rate: 5 mV/s): (a) pure titanium, (b) amorphous TiO<sub>2</sub> nanoarray tube, (c) anatase TiO<sub>2</sub> nanoarray tube, and (d) anatase Zr/TiO<sub>2</sub> nanotube array electrode; nanoarray tube, (e) the influence of concentrations of Zr(NO<sub>3</sub>)<sub>4</sub> solution in chemical immersion process; (f) schematic illustration of electrocatalytic reduction mechanism of the anatase Zr/TiO<sub>2</sub> nanotube array electrode for L-cystine.

#### 4. Conclusions

The Zr<sup>4+</sup>-doped anatase TiO<sub>2</sub> nanotube array electrode was prepared through anodizing, combined with chemical immersion and heat treatment. Zr<sup>4+</sup>-doping into the anatase TiO<sub>2</sub> induces the transformation of Ti<sup>4+</sup> to Ti<sup>3+</sup> and the formation of the oxygen vacancies, improving the electrocatalytic activity of the as-prepared electrode for L-cysteine reduction.

**Author Contributions:** Conceptualization, X.Z. (Xuhui Zhao) and Y.T.; methodology, W.W.; investigation, G.W.; writing—original draft preparation, W.W.; writing—review and editing, X.Z. (Xuhui Zhao) and Y.T.; **Author Contributions:** Conceptualization, X.Z. (Xuhui Zhao) and Y.T.; methodology, W.W.; investigation, G.W.; visualization, W.W. and G.W.; supervision, Y.Z. and X.Z. (Xiaofeng Zhang); funding acquisition, X.Z. (Xuhui



writing—original draft preparation, W.W.; writing—review and editing, X.Z. (Xuhui Zhao), and Y.T.; visualization, Zhao). All authors have read and agreed to the published version of the manuscript.

W.W. and G.W.; supervision, Y.Z. and X.Z. (Xiaofeng Zhang); funding acquisition, X.Z. (Xuhui Zhao). All authors have read and agreed to the published version of the manuscript. This research was funded by the National Key Research and Development Program of China, grant number 2017YFB0307500.

**Funding:** This research was funded by the National Key Research and Development Program of China, grant number 2017YFB0307500.

**Conflicts of Interest:** The authors declare no conflict of interest.

**Conflicts of Interest:** The authors declare no conflict of interest.

**References** 1. Ralph, T.R.; Hitchman, M.L.; Millington, J.P.; Walsh, F.C. The reduction of L-cystine hydrochloride at stationary and rotating disc mercury electrodes. *Electrochim. Acta* **2005**, *51*, 133–145.

1. Ralph, T.R.; Hitchman, M.L.; Millington, J.P.; Walsh, F.C. The reduction of L-cystine hydrochloride at stationary and rotating disc mercury electrodes. *Electrochim. Acta* **2005**, *51*, 133–145. [\[CrossRef\]](#)
2. Yang, S.; Li, G.; Liu, L.; Wang, G.; Wang, D.; Qu, L. Preparation of nickel oxide nanoparticles on N-doped reduced graphene oxide: A two-dimensional hybrid for electrocatalytic sensing of L-cysteine. *J. Alloy. Comp.* **2017**, *691*, 834–840. [\[CrossRef\]](#)
3. Nosal-Wiercinska, A. The catalytic activity of cysteine and cystine on the electroreduction of Bi(III) ions. *J. Electroanal. Chem.* **2011**, *662*, 298–305. [\[CrossRef\]](#)
4. Wei, M.; Guo, J.; Shi, Z.; Yuan, Q.; Pu, M.; Rao, G.; Duan, X. Preparation and characterization of L-cystine and L-cysteine intercalated layered double hydroxides. *J. Mater. Sci.* **2007**, *42*, 2684–2689. [\[CrossRef\]](#)
5. Ke, D.; Liu, H.; Peng, T.; Liu, X.; Dai, K. Preparation and photocatalytic activity of WO<sub>3</sub>/TiO<sub>2</sub> nanocomposite particles. *Mater. Lett.* **2008**, *62*, 447–450. [\[CrossRef\]](#)
6. Kment, S.; Riboni, F.; Pausova, S.; Wang, L.; Wang, L.Y.; Han, H.; Hubicka, Z.; Krysa, J.; Schmuki, P.; Zboril, R. Photoanodes based on TiO<sub>2</sub> and -Fe<sub>2</sub>O<sub>3</sub> for solar water splitting—superior role of 1D nanoarchitectures and of combined heterostructures. *Chem. Soc. Rev.* **2017**, *46*, 3716–3769. [\[CrossRef\]](#)
7. Qin, P.; Paulose, M.; Ibrahim Dar, M.; Moehl, T.; Arora, N.; Gao, P.; Varghese, O.K.; Grätzel, M.; Nazeeruddin, M.K. Stable and efficient perovskite solar cells based on Titania nanotube arrays. *Small* **2015**, *11*, 5533–5539. [\[CrossRef\]](#)
8. Liang, X.P.; Lian, Z.W.; Zhu, J.; Men, K.; Wei, F. The preparation and properties of TiO<sub>2</sub> nano-porous layers for perovskite solar cells. *AIP Adv.* **2020**, *10*, 015058. [\[CrossRef\]](#)
9. Ozkan, S.; Ghanem, H.; Mohajernia, S.; Hejazi, S.; Fromm, T.; Borchardt, R.; Rosiwal, S.; Schmuki, P. Boron-doped diamond as an efficient back contact to thermally grown TiO<sub>2</sub> photoelectrodes. *ChemElectroChem* **2019**, *6*, 4545–4549. [\[CrossRef\]](#)
10. Zhang, Y.; Pan, C. TiO<sub>2</sub>/graphene composite from thermal reaction of graphene oxide and its photocatalytic activity in visible light. *J. Mater. Sci.* **2011**, *46*, 2622–2626. [\[CrossRef\]](#)
11. Zhang, W.; Shironita, S.; Umeda, M. Low Pt loading and high hydrogen oxidation reaction performance at Pt/TiO<sub>2</sub>–SiO<sub>2</sub> investigated by a porous microelectrode. *Catal. Lett.* **2014**, *144*, 112–116. [\[CrossRef\]](#)
12. Skúlason, E.; Bligaard, T.; Gudmundsdóttir, S.; Studt, F.; Rossmeisl, J.; Abild-Pedersen, F.; Vegge, T.; Jónsson, H.; Nørskov, J.K. A theoretical evaluation of possible transition metal electro-catalysts for N<sub>2</sub> reduction. *Phys. Chem. Chem. Phys.* **2012**, *14*, 1235–1245. [\[CrossRef\]](#) [\[PubMed\]](#)

13. Hirakawa, H.; Hashimoto, M.; Shiraishi, Y.; Hirai, T. Photocatalytic conversion of nitrogen to ammonia with water on surface oxygen vacancies of titanium dioxide. *J. Am. Chem. Soc.* **2017**, *139*, 10929–10936. [[CrossRef](#)] [[PubMed](#)]
14. Chen, X.B.; Liu, L.; Yu, P.Y.; Mao, S.S. Increasing solar absorption for photocatalysis with black hydrogenated titanium dioxide nanocrystals. *Science* **2011**, *331*, 746–750. [[CrossRef](#)] [[PubMed](#)]
15. Song, L.; Zhang, R.; Zang, S.; He, H.; Su, Y.; Qiu, W.; Sun, X. Activity of selective catalytic reduction of NO over V<sub>2</sub>O<sub>5</sub>/TiO<sub>2</sub> catalysts preferentially exposed anatase {001} and {101} facets. *Catal. Lett.* **2017**, *147*, 934–945. [[CrossRef](#)]
16. Krbal, M.; Sopha, H.; Pohl, D.; Benes, L.; Damm, C.; Rellinghaus, B.; Kupčik, J.; Bezdička, P.; Šubrt, J.; Macak, J.M. Self-organized TiO<sub>2</sub> nanotubes grown on Ti substrates with different crystallographic preferential orientations: Local structure of TiO<sub>2</sub> nanotubes vs. photo-electrochemical response. *Electrochim. Acta* **2018**, *264*, 393–399. [[CrossRef](#)]
17. Saputera, W.H.; Mul, G.; Hamdy, M.S. Ti<sup>3+</sup>-containing titania: Synthesis tactics and photocatalytic performance. *Catal. Today* **2015**, *246*, 60–66. [[CrossRef](#)]
18. Cao, N.; Chen, Z.; Zang, K.; Xu, J.; Zhong, J.; Luo, J.; Xu, X.; Zheng, G. Doping strain induced bi-Ti<sup>3+</sup> pairs for efficient N<sub>2</sub> activation and electrocatalytic fixation. *Nat. Commun.* **2019**, *10*, 2877. [[CrossRef](#)]
19. Shi, M.M.; Bao, D.; Wulan, B.R.; Li, Y.H.; Zhang, Y.F.; Yan, J.M.; Jiang, Q. Au sub-nanoclusters on TiO<sub>2</sub> toward highly efficient and selective electrocatalyst for N<sub>2</sub> conversion to NH<sub>3</sub> at ambient conditions. *Adv. Mater.* **2017**, *29*, 1606550. [[CrossRef](#)]
20. Lucky, R.A.; Charpentier, P.A. N-doped ZrO<sub>2</sub>/TiO<sub>2</sub> bimetallic materials synthesized in supercritical CO<sub>2</sub>: Morphology and photocatalytic activity. *Appl. Catal. B Environ.* **2010**, *96*, 516–523. [[CrossRef](#)]
21. Reddy, M.V.; Sharma, N.; Adams, S.; Rao, R.P.; Peterson, V.K.; Chowdari, B.V.R. Evaluation of undoped and M-doped TiO<sub>2</sub>, where M = Sn, Fe, Ni/Nb, Zr, V, and Mn, for lithium-ion battery applications prepared by the molten-salt method. *RSC Adv.* **2015**, *5*, 29535. [[CrossRef](#)]
22. Macak, J.M.; Gong, B.G.; Hueppe, M.; Schmuki, P. Filling of TiO<sub>2</sub> nanotubes by self-doping and electrodeposition. *Adv. Mater.* **2010**, *19*, 3027–3031. [[CrossRef](#)]